JOURNAL OF CATALYSIS 78, 289–305 (1982)

Pt/SiO_2

VI. The Effects of Pretreatment on Structures

R. K. NANDI, F. MOLINARO, C. TANG, J. B. COHEN,[1] J. B. BUTT, AND R. L. BURWELL, JR.

Department of Materials Science & Engineering, The Technological Institute and Ipatieff Catalytic Laboratory, Northwestern University, Evanston, Illinois 60201

Received February 5, 1982; revised June 7, 1982

Pt catalysts with a wide range of percentage metal exposed have been examined by wide-angle and small-angle X-ray scattering, extended X-ray absorption fine structure (EXAFS), and X-ray fluorescence. The wide-angle studies were carried out in a special cell that permitted treatment in a gas environment at moderate temperatures. For high percentage metal exposed, the wide-angle patterns (as well as all EXAFS spectra) were obtained with X rays from the storage ring at Cornell University. After exposure to air, a catalyst with 63.5% Pt exposed consists of particles of crystalline Pt_3O_4 with a core of Pt, whereas for 81% exposed, the catalyst is nearly fully oxidized. There is no indication of any difference between the Pt–Pt distance in these catalysts and that in bulk Pt, nor is there any difference for 40% exposed or less (for which the exposed catalyst is Pt metal), even after reductions in H_2. There is little contact area between the catalyst and the support. For the lowest percentage metal exposed (6.3%), reductions in hydrogen do not change the microstrains within particles, but there is reduction in particle size, which is greater the higher the reduction temperature. The activity of this catalyst decreases in the same manner. The mean-square amplitude of vibration increases with the temperature of H_2 reduction for several catalysts, as does the catalytic activity.

INTRODUCTION

In this series of papers (*1–5*), we have examined well-characterized Pt/SiO_2 catalysts, using chemical techniques and X-ray diffraction. Up to 40% metal exposed, wide-angle X-ray diffraction (WAXS) showed that the catalyst was Pt metal, with a lattice parameter identical to that of the bulk, even after long storage in air (*2*). The particles of Pt were quite perfect, except those of a size similar to the size of the pores in the silica gel support (6.3% Pt exposed). There was good agreement between the percentage Pt exposed determined from the crystallite size with X rays, D_x, and that determined with pulsed H_2 chemisorption at 25°C, D_h (*1*). For D_h greater than 40%, the diffraction pattern could not be detected with normal X-ray sources. However, the O/Pt ratio for the catalysts with $D_h = 81\%$, exposed to air at room temperature, was 0.89 (*1*). Some authors (*6–8*) have reported that the extended X-ray absorption fine structure (EXAFS) patterns of such highly dispersed catalysts at room temperature in air or oxygen indicate that they involve amorphous oxides of the formula PtO_2 (*6, 7*) or PtO (*8*). However, the measured O/Pt ratio appears too low for PtO_2 to be correct.

It was also shown in this series (*3*) that there was a good correlation between turnover frequency and vibrational amplitude determined from WAXS, the catalytic activity increasing linearly with amplitude. Subsequently (*5*), we showed that the temperature of H_2 reduction in the pretreatment of these catalysts strongly affected the turnover frequency for the formation of iso- and normal butane products during hydrogenolysis of methylcyclopropane. The

[1] To whom correspondence should be addressed.

0021-9517/82/120289-17$02.00/0

structure sensitivity can be reversed or minimized by such pretreatment. This effect affords us an unusual opportunity to test the role of vibrational amplitude.

Therefore, the purpose of this paper is threefold; first we reexamine the nature of Pt catalyst stored in air, with particular attention to high dispersions. Then we examine the effect of H_2 pretreatment. The techniques employed include EXAFS, WAXS, small-angle X-ray scattering (SAXS), and X-ray fluorescence. Finally, the correlation between vibrational amplitude and catalytic activity is examined after various H_2 pretreatments.

In the course of this study we have developed simple procedures suitable for obtaining diffraction patterns from catalysts in controlled atmospheres, and these will be described.

EXPERIMENTAL PROCEDURES

Treatment of Catalysts

The catalysts are listed in Table 1; details on their preparation can be found in Ref. (*1*). A gas train was constructed to allow treatment with O_2, He, or H_2 gas, at various temperatures. Each line had a U-tube trap filled with silica gel, and those used for H_2 and He were immersed in liquid nitrogen to minimize oxygen or water vapor. For the O_2 line, a dry-ice–alcohol trap was employed to minimize water vapor. Each line was equipped with an on–off valve for the manifold to the specimen holder, and a needle valve to control the flow rate. The pressure from the main supply tanks was kept at 10 psi to avoid damage to the window on the sample holder. A desired temperature during pretreatment was obtained by placing an open-ended cylindrical furnace over the tubular section of the specimen holder. (The furnace was a 3.8-cm-diameter mullite tube, wound with Kanthal A-1 wire.) Temperature was measured with a Chromel–Alumel thermocouple.

TABLE 1

Pt Catalysts, D_h, and Metal Loading during Preparation

Catalyst[a]	D_h (%)	Metal loading (wt%)
6.3-SiO_2-PtCl-L	6.3	1.97
21.5-SiO_2-IonX-L	21.5	1.17
40-SiO_2-PtCl-S	40	1.49
63.5-SiO_2-IonX-L	63.5	0.49
81-SiO_2-IonX-S	81	0.83

[a] The first number is percentage exposed from H_2 chemisorption, followed by the support, method of including Pt (IonX = ion exchange, with $Pt(NH_3)_4Cl_2$; PtCl = impregnation with H_2PtCl_6). The last symbol: L = 70–80 mesh, S = 120–140 mesh (for gel).

The glass sample cell, mounted on a diffractometer, is shown in Fig. 1. One valve shown provides the connection to the gas train, whereas the other connects to a flowmeter. Catalyst is poured into the tubular section via the vertical flow valve, and is maintained in this section during pretreatment. The cell is then tipped to move the powder into the circular section, which is 0.6 cm thick, 4 cm in diameter, with a 0.001-cm mica window sealed to the glass with Torr Seal. The cell holds approximately 3.5 g of catalyst.

To check the cell for leakage, it is periodically loaded with 10–15% MnO supported on silica gel, which is then reduced in H_2 at 350–450°C for 30 min, and cooled in H_2. The green oxide turns brown on exposure to oxygen, with a detection limit of about 0.5 ppm. When the cell is properly sealed, no color change is observed, even after 1 week at room temperature.

A cell for examining the diffraction pattern in controlled atmospheres has also been described by Borodzinski and Janko (*9*). In contrast to that system, the one described here holds considerably more catalyst under the X-ray beam, so that typical metal loadings yield usable diffraction patterns. (In another paper (*10*), we have described a sample cell for observing the diffraction pattern *during* gas treatment or a catalytic reaction, rather than the batch process described here. However, much smaller quantities of catalyst were em-

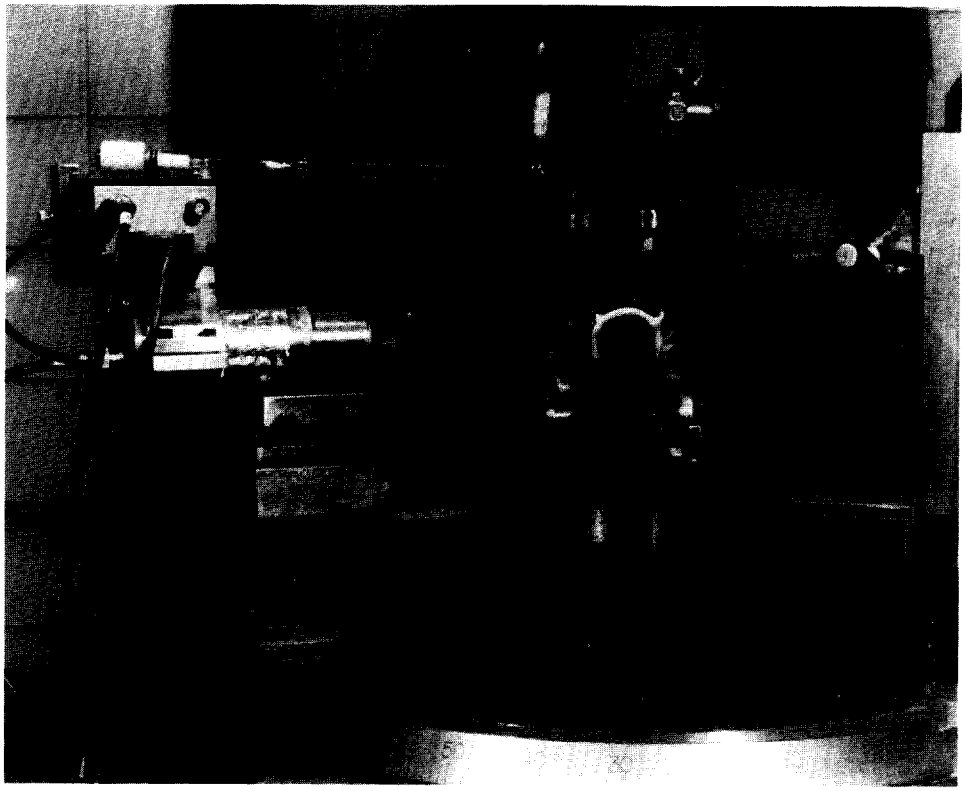

FIG. 1. Glass sample cell on a diffractometer. The catalyst is in the circular section. It is loaded through the vertical valve to the left of this section. Heat treatments are carried out with the catalyst in the long horizontal tube, connected to the gas train through the valve on the far left.

ployed in this cell, and higher metal loadings were required for the low-D_h catalysts studied.)

The actual treatments performed on the catalysts (after storage in air for a year or more) are indicated in Table 2. All treatments were performed on the same batch of catalyst, sequentially, without exposure to air. The inlet valve of the cell was closed after each treatment and the cell was moved from the furnace to the diffractometer. The standard pretreatment is designated as "A." Before each reduction, a sample was reoxidized at 300°C for 30 min. A purge of He for 15 min was employed between treatments with O_2 and H_2. All gas flow rates were typically 25–30 cm^3/min. (The purge was with Ar for measurements of D_h, but with He for the X-ray studies, because of its lower X-ray absorption.)

TABLE 2

Pretreatments

Run	Conditions
A	O_2, 300°C, 0.5 hr; H_2, 300°C, 1 hr; heat to 450°C, 1 hr, and cool to 25°C, all in He
B	O_2, 300°C, 0.5 hr; H_2, 25°C, 1 hr
C	O_2, 300°C, 0.5 hr; H_2, 200°C, 1 hr; cool to 25°C in H_2
D	O_2, 300°C, 0.5 hr; H_2, 450°C, 1 hr; cool to 25°C in H_2
E	O_2, 300°C, 0.5 hr; He, 450°C, 1 hr; cool to 25°C in He

WAXS

For the catalysts with $D_h \leq 50\%$, the automated point-counting procedure described in Ref. (*2*) was employed here, with Ni-filtered Cu$K\alpha$ radiation from a sealed X-ray tube operated at 50 kV, 11 mA. The receiving slit was 0.2° wide (without a Soller slit) and the divergence in the incident beam was 1° for $2\theta < 75°$ and 3° for $2\theta > 75°$.

The principal procedure for obtaining information from the wide-angle diffraction pattern was Fourier analysis of peak shape. Information on microstrains, crystallite size, and size distribution is obtained from the coefficients of the Fourier series representing a diffraction peak, after these are corrected for broadening due to the geometry of the experiment. These coefficients are obtained vs L, a distance normal to the diffracting planes. If these coefficients superimpose for first- and second-order peaks, there are no microstrains. If there are such strains, the coefficients decrease more rapidly for the second-order peak than for the first-order peak. After correcting for the effects of such strains, the initial slope of the coefficients vs L yields the average crystallite size P_s, while the second derivative gives the size distribution $P(L)$. More details can be found in Ref. (*2*).

A volumetric mean particle size ($\bar{P}_s$) can be obtained from the relationship

$$\bar{P}_s = \sum_L LP(L)\,\Delta L, \qquad (1)$$

after normalizing the fraction of size L, $P(L)$.

From the average crystallite size (in different crystallographic directions) the percentage exposed, D_x, can be calculated (*1*) as

$$D_x = \frac{11.26}{P_s} \times 100 \qquad (2)$$

This can then be compared to percentage metal exposed from pulsed H_2 chemisorption, D_h.

The volume fraction of the metal phase of the supported catalysts can be obtained (*11*) by comparison of the integrated intensity (I) of a peak and that of a standard of known volume fraction (C). Let 1 denote the standard, 2 the unknown Pt on silica gel:

$$\frac{I_1^{Pt}}{I_2^{Pt}} = \frac{C_1^{Pt}C_2^{Pt}\left(\mu_{Pt} - \mu_{SiO_2}\right) + C_1^{Pt}\mu_{SiO_2}}{C_1^{Pt}C_2^{Pt}\left(\mu_{Pt} - \mu_{SiO_2}\right) + C_2^{Pt}\mu_{SiO_2}}. \qquad (3)$$

As I_1 and I_2 are measured, C_1 is known, and the linear absorption coefficients are tabulated, C_2 can be obtained. Then the weight fraction ω can be calculated:

$$C_2^{Pt} = [\omega_2^{Pt}/\rho_{Pt}]\,[\omega_2^{Pt}/\rho_{Pt} + \omega_2^{SiO_2}/\rho_{SiO_2}]^{-1}, \qquad (4)$$

where the ρ's are the respective densities.

For standards, known amounts of Pt black were mixed with supports: 1.97 wt% Pt in SiO_2 and 3 wt% Pt in Al_2O_3. The absorption coefficients were taken from Ref. (*12*) and the densities form Refs. (*13*, *14*).

The accuracy in crystallite sizes is estimated to be ~10% for sizes greater than 50 Å and ~15% for smaller sizes. The error in microstrain is $\pm 0.2 \times 10^{-3}$ and in weight percentage, 0.15. These errors were estimated by repeated measurements on similar samples.

Information on lattice parameters and mean-square amplitudes of vibration was obtained as in Ref. (*2*), using Zr-filtered Mo$K\alpha$ radiation from a Rigaku rotating-anode generator operated at 50 kV and 180 mA; 111, 220, 311, 222, 400, 422, and 333/511 peaks were integrated for the calculations.

Highly dispersed catalysts with $D_h > 50\%$ were examined in air using X rays from the Cornell High Energy Synchrotron Source (CHESS), Ithaca, New York. X rays of a wavelength close to that of Cu$K\alpha$ were obtained by using an elastically bent, thin triangular Si crystal, cut to expose (111) planes. Subharmonic wavelengths

were eliminated by total reflection from a float-glass mirror. The direct beam was monitored constantly with a flowing-N_2 gas ion chamber and the diffracted photons were counted with a scintillation detector.

SAXS

Small-angle scattering patterns were collected on a Rigaku-Denki slit system, coupled to a one-dimensional position-sensitive detector and multichannel analyzer. Zr-filtered Mo$K\alpha$ radiation from a rotating-anode generator operated at 30 kV, 10 mA was employed. The thickness of the samples was μ^{-1}, where μ is the linear absorption coefficient of the sample. The data were corrected for parasitic scattering obtained by replacing a specimen with a blank specimen holder, with the same Mylar sheets used to retain the catalyst. These data were also corrected for absorption by standard calculations.

The method recently proposed by Goodisman *et al.* (*15*) for the determination of the various surface areas in a supported metal catalyst was followed. This method has the principal advantage of not requiring any liquid pore maskant. In the results, the subscripts 1, 2, 3 designate the three phases, support, void, and metal, and the bracketed superscripts 2, 3 designate, respectively, the two-phase (support–void) and the three-phase (support–void–metal) systems. Thus $S_{31}^{(3)}$ is the surface area between metal and support in the catalyst.

The SAXS data were processed on a minicomputer.

X-Ray Fluorescence

The lines of Pt produced by Zr-filtered Mo$K\alpha$ radiation from a Rigaku rotating-anode generator were observed with a Si (LI) solid-state detector. The integrated intensities of these lines were obtained at 25° 2θ, well away from the Bragg peaks from Pt.

EXAFS

The oscillations in intensity above the L edge of Pt were observed with X rays from CHESS. The energy was varied with a channel-cut Si crystal. The sample thickness was approximately 1.6μ, and the incident and transmitted intensities were measured with an 8-cm-long flowing-N_2 ion chamber and a 30-cm flowing-argon chamber, respectively. The absorption below the absorption edge was fitted to a Victoreen formula, and extrapolated above the edge to provide $\mu_B(E)$. A similar fit was made above the edge to three points so that the curve passed smoothly through the oscillations. Subsequently, the oscillations were smoothed by iterative averaging of groups of three neighboring points at intervals of 5–15 eV to obtain $\mu_0(E)$. Let E_s represent the energy at the beginning of the EXAFS region; then the oscillations $\chi(E)$ (above the edge), around the smooth variation in μ, are obtained from

$$\chi(E) = \frac{\mu_{raw}(E) - \mu_0(E)}{[\mu_0(E_s) - \mu_B(E_s)](E_s/E)^3}. \quad (5)$$

The cubed term in the denominator accounts for the variation in μ with E above E_s. The relation among the incident energy, E, the wave vector of the photoelectron, k, and the energy at the absorption edge, E_0, is

$$k = \left(\frac{2m}{h^2}(E - E_0)\right)^{1/2}. \quad (6)$$

Then (*16, 17*),

$$\chi(k) = \sum_j \left(\frac{N_j}{kR_j^2} F_j(k)\right) e^{-2\sigma_j^2 k^2} e^{-2R_j/\lambda} \sin(2kR_j + \varphi(k)), \quad (7)$$

where

N_j = number of neighboring atoms in the jth coordination shell,
R_j = neighbor distance of jth-type atom,
σ_j = Debye–Waller factor for jth-type atom,
λ = electron mean free path,

F_j = backscattering amplitude for jth-type atom,

$\varphi_j^{(k)}$ = sum of phase shifts on electron emission from the absorbing atom, and backscattering from the jth neighbor.

After multiplying $\chi(k)$ by k^3 to magnify small oscillation at large k, and by a Gaussian-broadened square window to minimize termination errors, the result was transformed to obtain the radial distribution function. Inverse Fourier transforms were then obtained of a particular neighbor shell. In this step, we were aided by simulation with models, to determine which side lobes to a peak were due to truncation due to the finite limits of the data, and should therefore be included in the back-transform. The resultant $k^3\chi(k)$ (for a single shell or a set of models, using theoretical values (*18*) for the backscattering amplitudes and phase shifts. The values thus obtained were N_j, R_j, σ_j, λ_j in Eq. (7) and the shift in E_0, ΔE_0.

RESULTS AND DISCUSSION

The Catalysts after Storage in Air

We have already shown (*2*) that for $D_h \leq 40\%$ the catalysts consisted of particles of Pt metal. For higher dispersions, it was necessary to obtain the wide-angle diffraction patterns with the intense X rays at CHESS, for which the beam was approximately one order of magnitude greater in intensity than the characteristic line from the 12-kW rotating-anode X-ray generator. For $D_h = 63.5\%$, a single peak was detected at $2\theta = 35.8°$, and for $D_h = 81\%$ at 35.9° 2θ. For the wavelength employed, and for Pt_3O_4 (*19*), there is one strong peak expected at 35.24°, for PtO (*20, 21*), 33.42°, and for PtO_2, two strong peaks would be expected at 27.2 and 34.08° 2θ (*22*). For Pt, the most intense peak, the 111 (which is also the first peak in the pattern), is at 39° 2θ. The existence of a peak at 35.8° strongly points to the presence of crystalline Pt_3O_4, *not* amorphous β-PtO_2, as had been previously suggested (*6, 7*). This is also more in keeping with the measured O : Pt ratio of 0.89 (*1*). The results cannot be explained by contracted cubo-octahedral or icosahedral particles (*8*) of Pt which would give diffraction peaks at angles higher than that for bulk Pt. Furthermore, Fourier analysis of peak shape gave particle sizes of 16 and 14 Å for $D_h = 63.5$ and 81%, which yields $D_x = 70$ and 81%, in good agreement with D_h. To verify this result, the EXAFS patterns from these two catalysts were measured. The $\chi(k)$ vs k are shown in Fig. 2. The rapid decay in the oscillations with increasing energy is unlike that for bulk Pt or for Pt/SiO_2 catalysts of lower dispersions (as will be shown later) and, in fact, is known to be a characteristic of an oxide (*6, 7*). The radial distribution functions (RDFs) are shown in Fig. 3. The main peak[2] is at a distance about 1 Å lower than that for Pt–Pt first neighbors. There is a small peak at ~2.5 Å for the 63.5% Pt exposed, which corresponds to Pt–Pt first neighbors in the metal. Its absence for $D_h = 81\%$ suggests that this catalyst is nearly completely oxidized.

For PtO, each Pt is surrounded by four oxygen atoms at 2.02 Å (*20, 21*), whereas for Pt_3O_4 (*19*), there are four oxygens at 1.97 Å and for β-PtO_2 (*22*), there are six oxygens, four at 1.98 Å and two at 2.02 Å. A nonlinear least-squares fit to the back-transformed first shell in Fig. 3 has been attempted for these structures. The fit for PtO or Pt_3O_4 (whose near-neighbor oxygen distances are within the experimental error for EXAFS) is shown in Fig. 4. The parameters are given in the first row of Table 3. The fit to the β-PtO_2 structure was rejected, because the value of λ was greater than 6, which is unusually high compared to literature values, and because WAXS indicated Pt_3O_4.

A fit for $D_h = 63.5\%$, including the small Pt peak in the RDF, is also shown in Table 3, and in Fig. 5. In this case, if λ is chosen to be the same value as for $D_h = 81\%$, N_1 =

[2] The distance scale is uncorrected for the phase shifts in Eq. (7).

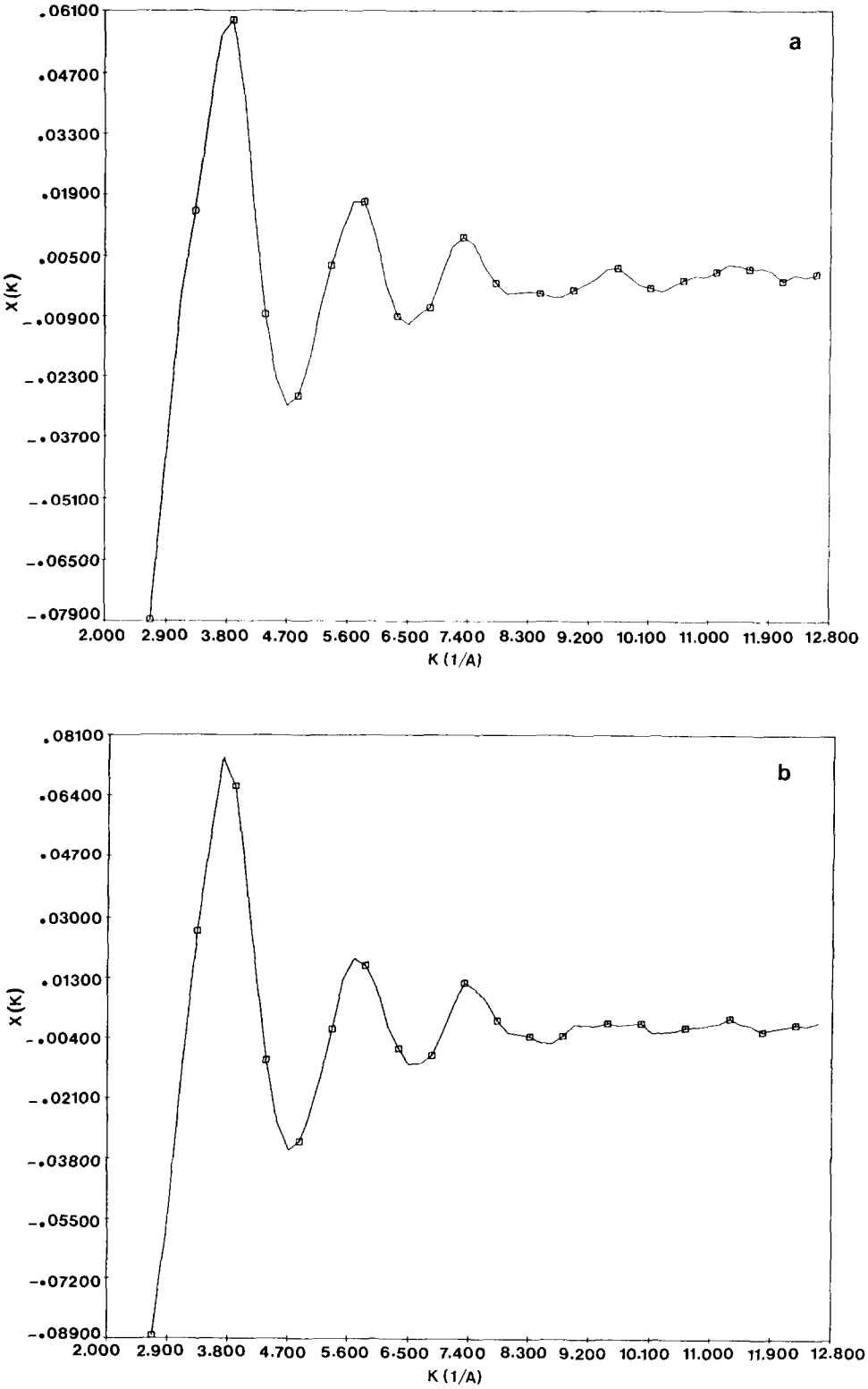

FIG. 2. $\chi(k)$ vs k: (a) $D_h = 63.5\%$, (b) $D_h = 81\%$. (Not all data points are shown.)

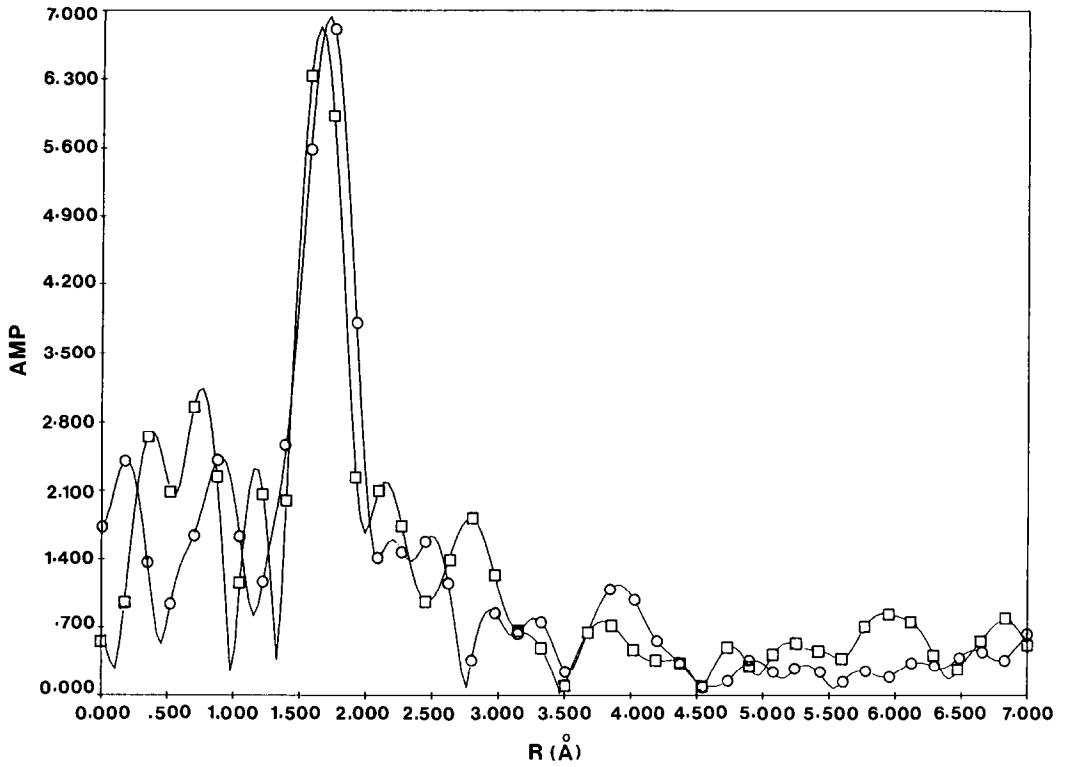

FIG. 3. RDF from Fig. 2 for D_h = 63.5% (□) and 81% (○).

2.8. This is within the usually accepted error (of ±20–30%) of the value of 3.4 in the table. However, the fact that both values are less than four for D_h = 63.5% (the number of oxygen first neighbors to Pt in Pt_3O_4) is probably because some Pt atoms do not have oxygen atoms in the first shell, but Pt instead, in a Pt metal core. Note also that the value of R_2 (the Pt–Pt distance) is 2.76 Å, essentially that for bulk Pt.

Thus we conclude that after storage in air these highly dispersed catalysts are primarily small crystallites of Pt_3O_4. For D_h = 63.5%, there is a small amount of Pt metal, probably present mainly in the larger particles. (For the measured O : Pt ratio of 0.89, and with the oxide Pt_3O_4, approximately one-third of the Pt atoms are in such metal cores. Their size would be 11–12 Å, at the limit of our ability to detect peaks in such dilute catalysts, even at CHESS.)

Effects of H_2 Pretreatment

The effect of the pretreatments in Table 2 on the turnover frequency and selectivity vs D_h for hydrogenolysis of methylcyclopropane are shown in Fig. 6. The effects of the various gas treatments, as observed from WAXS, are summarized in Table 4. (It is worth emphasizing here that the effects reported were verified by repeating the measurements two additional times on fresh catalysts.) Microstrain was detected only in the catalysts with D_h = 6.3%, that is, it is only for this catalyst that the Fourier coefficients of the two reflections, 111 and 222, do not superimpose. The value of the root-mean-square (rms) microstrain, $\langle \epsilon_L^2 \rangle^{1/2}$, at l = 50 Å, is 3×10^{-3}, quite similar to the value after storage in air reported in Ref. (*2*), and this was unaffected by the various treatments. The dislocation density

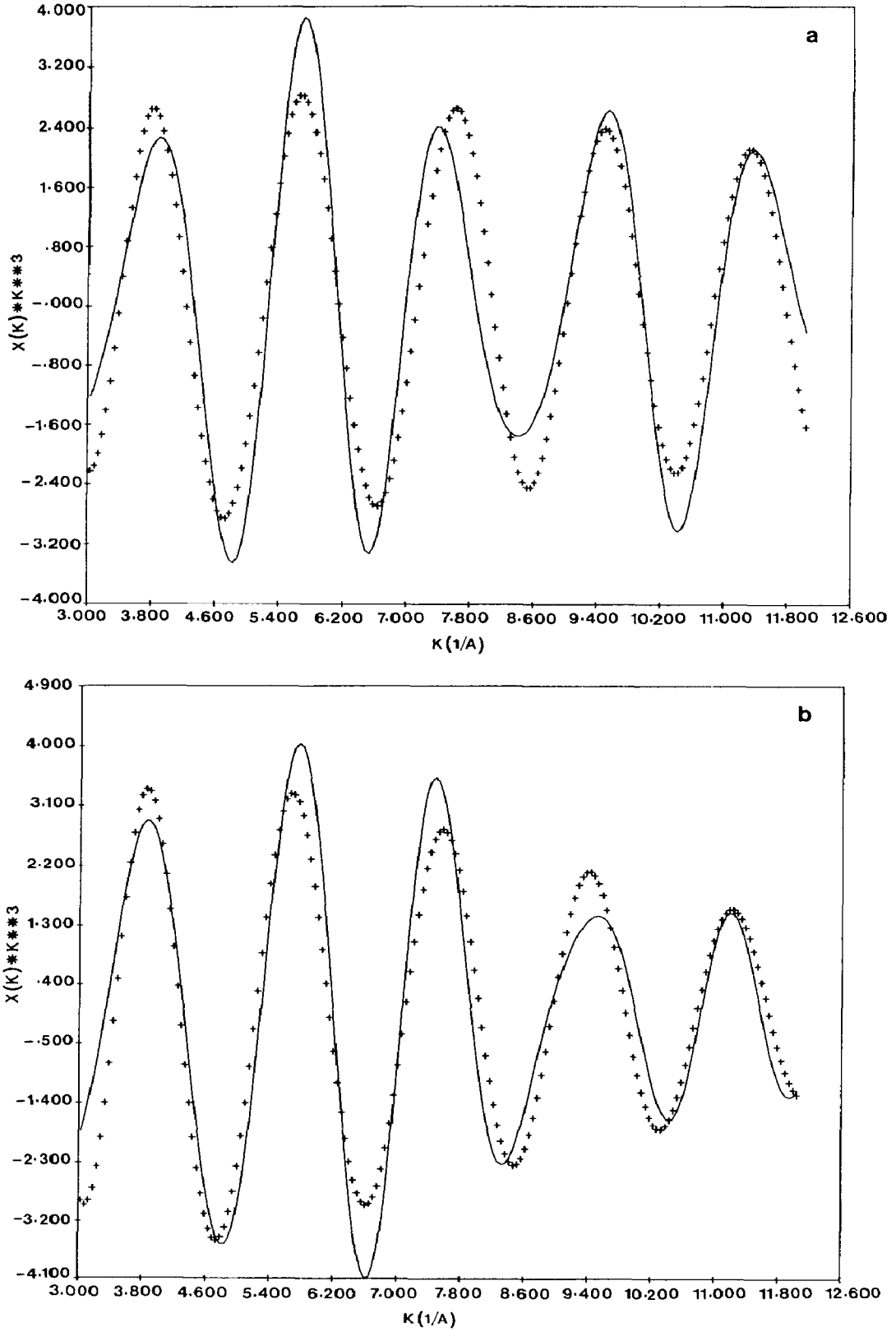

FIG. 4. $k^3\chi(k)$ vs k. First-shell back-transformation, and simulation (crosses) from results of the nonlinear least squares in Table 3 (for Pt_3O_4): (a) D_h = 63.5%, (b) D_h = 81%.

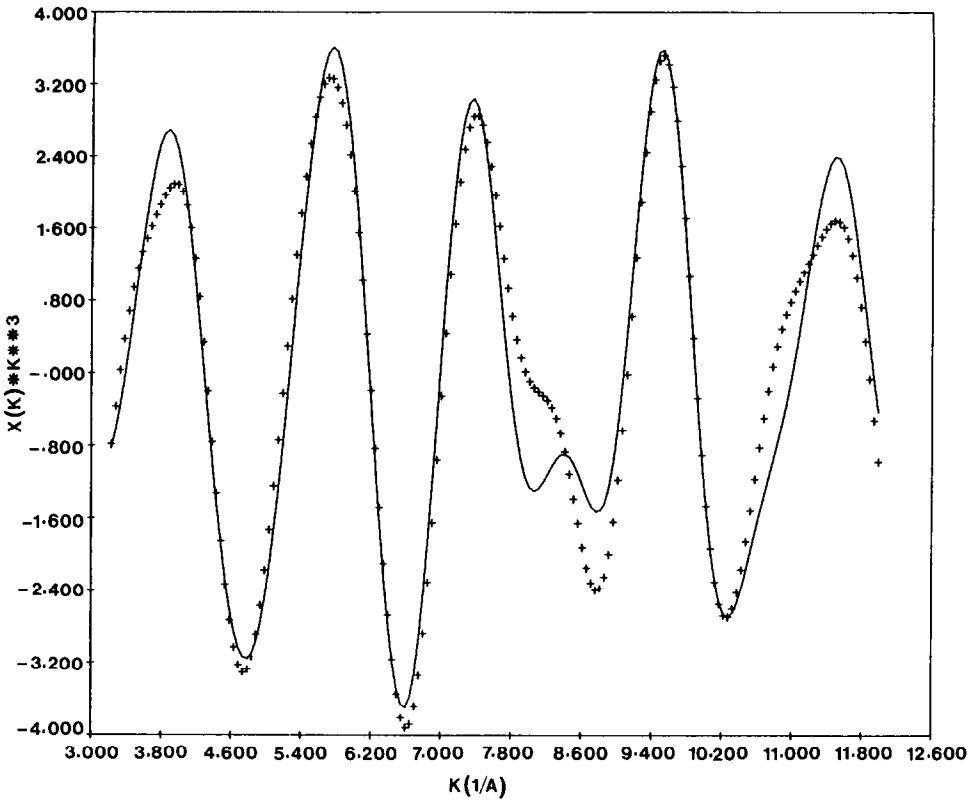

FIG. 5. $k^3\chi(k)$ vs k for back-transformation of main oxygen peak in RDF, and small Pt peak. Simulation (crosses) with the results of nonlinear least squares in Table 3. D_h = 63.5%.

corresponding to this strain amounts to 6×10^{11} dislocations/cm^2, a relatively high value, comparable to that in heavily deformed metals (see Ref. (*2*) for the relation linking these two quantities). The particle sizes after pretreatment A were, within experimental error, identical to those reported in Ref. (*2*) for the same catalysts stored in air. The primary effect of the successive reductions in H_2 at increasing temperatures is a reduction in the particle size and weight fraction of Pt but *only* for the catalyst 6.3-SiO_2-PtCl-L. This is curious because (see Fig. 6) this catalyst is more active for the hydrogenolysis of methylcyclopropane after pretreatment at a low temperature than after that at high temperatures.

In the size distributions, given in Fig. 7, it is noteworthy that there is a tail toward larger sizes for the catalysts with 21.5 and 40% exposed, but toward smaller sizes for the catalyst with 6.3% exposed. The only significant effect of the H_2 reductions on the size distributions occurs for the catalyst with 6.3% exposed: the fraction of larger sizes is reduced and that of smaller sizes increased in this case.

Other sequences of treatments were also carried out for D_h = 6.3%. Proceeding directly to run D after A with a fresh sample, without the intervening treatments, caused a similar drop in weight fraction as after the entire sequence A–D. The high-temperature treatment E did not return the catalyst to the state which had followed pretreatment A. In another sequence, after run A with a fresh sample, passing H_2 at 25°C (without the intervening 300°C treatment with O_2) caused a similar reduction in weight fraction as with the intervening step (run B). Finally, exposure to air after treat-

TABLE 3

Results of Nonlinear Least-Squares Fit to $k^3\chi(k)$ Corresponding to First Oxide Peak and the Oxide Peak Together with the Pt Peak

Sample	Condition	N_1	R_1 (Å)	λ_1 (Å)	σ_1^2 (10^{-3} Å^2)	$(\Delta E_0)_1$ (eV)	N_2	R_2 (Å)	λ_2 (Å)	σ_2^2 (10^{-3} Å^2)	$(\Delta E_0)_2$ (eV)	Root-mean-square residual[a]
63.5-SiO_2-IonX-L	Oxide peak	4 (fixed)	2.01	3.741	1.098	15.83						0.731
	Oxide peak + Pt peak	3.4	2.01	4.5 (fixed)	0.997	16.04	3.74	2.76	4.5 (fixed)	7.95	1.751	0.502
81-SiO_2-IonX-S	Oxide peak	4 (fixed)	2.03	5.658	3.719	17.88						0.665

[a] Fractional difference in observed back-transform and that calculated from values in the table.

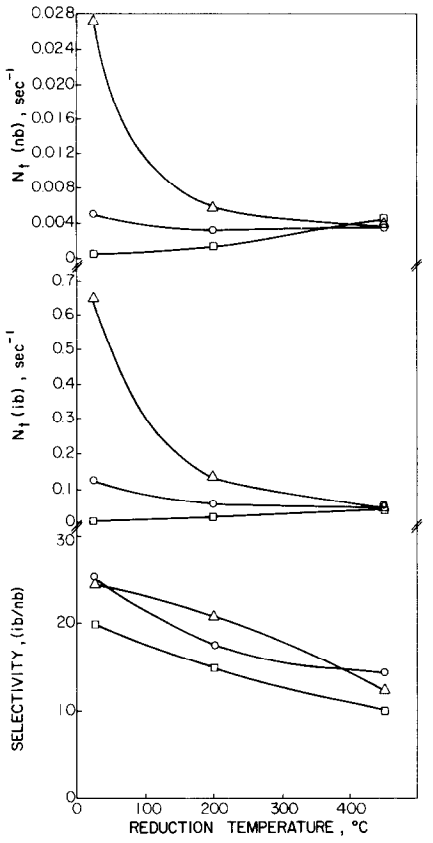

FIG. 6. Turnover numbers and selectivity for iso- and normal butane (ib and nb), during the hydrogenolysis of methylcyclopropane. ○: D_h = 6.3%; △: D_h = 21.5%; □: D_h = 40%.

ments A and D did not alter the integrated intensity, and therefore did not reconstruct the catalyst.

Perhaps the "loss" of Pt for D_h = 6.3% involves a reduction in particle size to sizes so small that they contribute primarily to the tails of diffraction peaks, which are difficult to detect precisely, due to the large scattering from the support. However, it is also possible that there is a real loss of Pt, or that the Pt dissolves in the support. Measurement of the X-ray fluorescence from Pt *L* lines showed that the Pt fluorescence after run D was only about 5% less than that after run A, whereas there was a 20–25% decrease in the area of a peak in WAXS. There is clearly no appreciable loss of Pt.

Even if the particles are as small as about

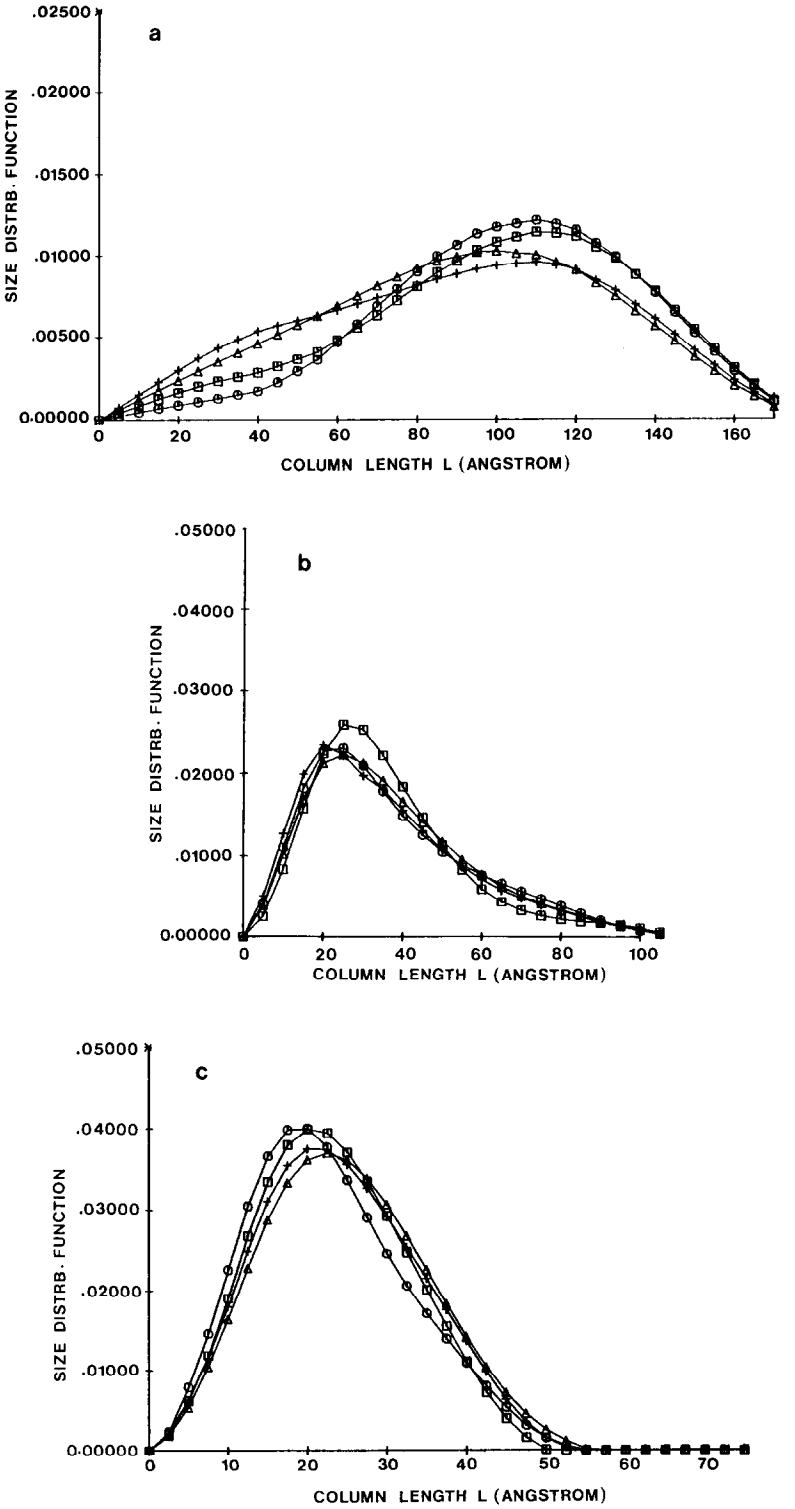

FIG. 7. Particle size distributions for Pt catalysts from WAXS: Probability of a given size vs size normal to the 111 diffracting planes. (a) D_h = 6.3%, (b) D_h = 21%, (c) D_h = 40%.

TABLE 4

Effects of Pretreatments on Pt/SiO_2 Catalysts

Catalyst	Treatment	Crystallite size (P_s) along ⟨111⟩ direction	$\langle \epsilon_L^2 = 50\ Å \rangle_{111}^{1/2}$ (10^{-3})	P_s[a] (Å)	D_x (%)	D_h (%)	Pt wt% from 111 peak	Loading during preparation (wt%)	Lattice parameter[b] (Å)
6.3-SiO_2-PtCl-L	A	105	2.28	101	11	6.3	1.60	1.97	3.9279 (12)
	B	102	2.82	103	11		1.40		3.9311 (12)
	C	96	2.73	92	12		1.34		3.9336 (17)
	D	93	3.10	91	12		1.20		3.9353 (10)
21.5-SiO_2-PtCl-L	A	39	0	36	29	21.5	1.55	1.49	3.9341 (35)
	B	38		37	30		1.51		3.9341 (18)
	C	38		37	30		1.49		3.9341 (25)
	D	37		36	30		1.54		3.9370 (30)
40-SiO_2-PtCl-S	A	24	0	23	47	40	0.92	1.17	3.9350 (72)
	B	24		23	47		1.01		3.9422 (82)
	C	25		25	45		0.98		3.9342 (82)
	D	25		24	45		1.01		3.9429 (74)

[a] Volumetric mean particle size obtained from the size distribution in Fig. 7 using relation (1).

[b] Lattice parameter of bulk Pt is 3.9239 Å (*20*). The values in parentheses are the observed standard deviations.

10Å, they should be detected by SAXS. However, the integrated small-angle scattering decreased by 25% after run D, compared to run A, so that we can only ascertain from the SAXS that the smaller particles are indeed quite small, or that some Pt dissolves in the support. The RDFs determined from EXAFS for $D_h = 6.3\%$ are shown in Fig. 8. There is no significant difference between treatments A and D. If Pt dissolved, peaks for Pt–O and/or Pt–Si distances should have been detected. Thus we must finally conclude that H_2 treatment does in fact produce quite small Pt particles. The Pt does not dissolve in the support.

We have previously reported (*1*) that treatment of 6.3-SiO_2-PtCl by pretreatment B led to substantially augmented values of percentage exposed of Pt as judged by subsequently exposing the catalyst to O_2 at 25°C followed by measurement of hydrogen consumption at 25°C. However, if the catalyst was treated in Ar at 450°C immediately after treatment B, the hydrogen consumption was normal, i.e., Ar at 450°C returned

TABLE 5

Results of Nonlinear Least-Squares Fit to $k^3\chi(k)$ Corresponding to First Coordination Shell[a]

Sample	R_1 (Å)	σ_1^2 (10^{-3} Å^2)	λ_1 (Å)	(ΔE_0) (eV)	Root-mean-square residual[b]
Pure Pt foil	2.756	3.153	5.673	1.84	0.876
6.3-SiO_2-PtCl-L	2.756	3.134	4.479	2.43	0.755
6.3-SiO_2-PtCl-L	2.759	3.327	4.596	3.00	1.059

[a] N_1 fixed at 12.

[b] Fractional difference in observed back-transform and that calculated from values in the table.

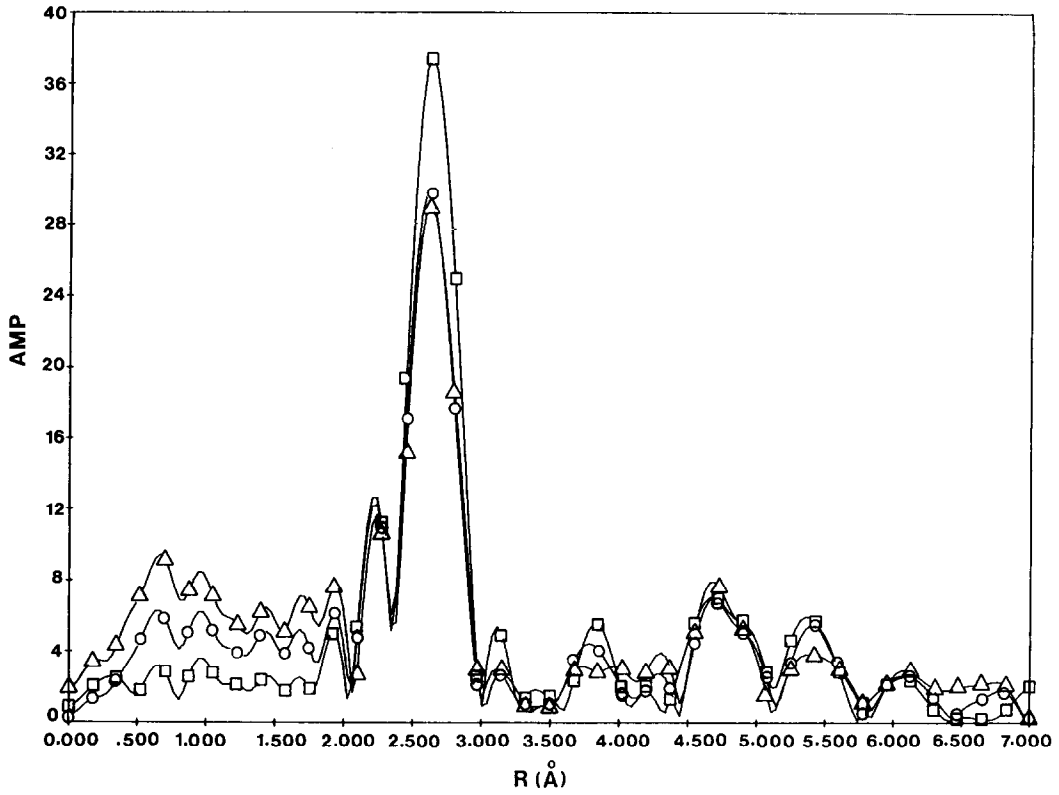

FIG. 8. RDF from EXAFS: Pure Pt foil (□); D_h = 6.3%: treatment A (○) and treatment D (△).

the percentage exposed, D_t (by hydrogen–oxygen titration), to its normal value.

We have now measured hydrogen adsorption at 25°C and hydrogen desorption at 450°C on a sample of 6.3-SiO_2-PtCl after each of the following sequential pretreatments: A (but Ar rather than He), repeat; B followed by Ar at 450°C, repeat; D followed by Ar at 450°C, repeat; A, repeat. All values of D_h were 6.9 ± 0.5 with no trend.[3] It appears, then, that Ar at 450°C restores catalysts given pretreatments B and D to the initial platinum particle size. At this point, we do not really understand the difference in the effect of pretreatments B, C, and D on 6.3-SiO_2-PtCl vs that on the 21.5 and 40% analogs.

The values of the various quantities in Eq. (7) obtained from these EXAFS patterns are presented in Table 5. An example of the fit to the first-shell data is shown in Fig. 9. If the λ value for the Pt foil is employed to fit the data on the catalysts, N_1 is ~9.3–9.5, rather than 12, the value for bulk Pt. Although the difference is about the accepted error for this quantity, the value expected from the size distributions in Fig. 7, following the calculations in Ref. (*23*), is N_1 = 10.1 for stored catalysts and N_1 = 10.4 after treatment B, close to the observed values. Note also from Table 5 that the first-neighbor Pt–Pt distance in the catalyst is that of bulk Pt, in agreement with the WAXS results, and with Ref. (*24*).

In Table 6 we give the results of the quantitative analysis of the SAXS data. The pore surface area is slightly larger than the BET value of 285 m^2/g. Particularly noteworthy is the fact that there is little interfacial area between the catalyst and the support (S_{31}). (We have also obtained a similar result from SAXS for a Pt-Al_2O_3 catalyst with D_h = 40%. With such a catalyst the

[3] This work was done by Dr. R. Pitchai.

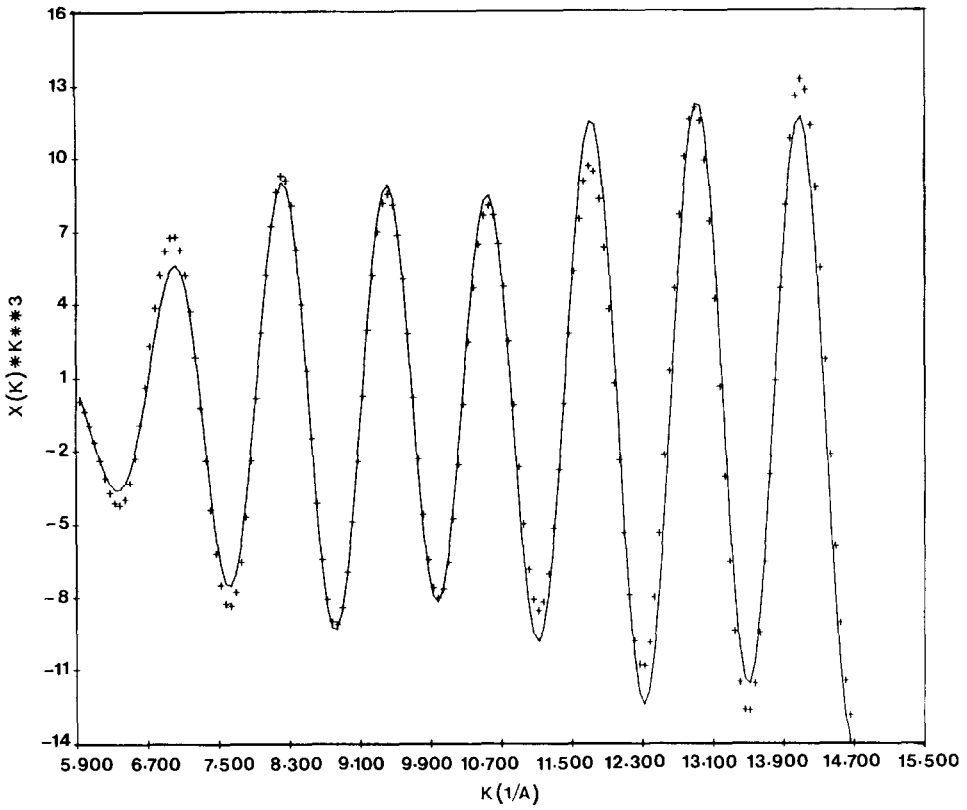

FIG. 9. Back-transformed $k^3\chi(k)$ for the first-neighbor shell, D_h = 6.3%, treatment D. Full curve from data; crosses are simulation with results of nonlinear least squares in Table 5.

alumina diffraction peaks interfere with most of those from Pt in WAXS, and SAXS is especially useful for characterization.)

Finally, from WAXS, it was also possible to determine the mean-square amplitude of vibration vs temperature of H_2 reduction. The results are shown in Fig. 10. The amplitude increases with pretreatment temperature. However, there is no simple correlation with the reactivity or selectivity given in Fig. 6. From this latter figure it can be seen that catalytic activity decreases with reduction temperature for some dispersions and increases for others. The selectivity de-

TABLE 6

SAXS, Platinum Catalysts

Sample	Condition	Volume fractions			S_{21}[a] (m^2/g)	S_{31}[a] (m^2/g)	S_{32}[a] (m^2/g)	S_{32}[b] (m^2/g)
		φ_1	φ_2	φ_3				
Silica gel (70–80 mesh)		0.1755	0.8245		327.4			
6.3-SiO_2-PtCl-L	Fresh	0.1754	0.8242	0.00036	323.9	0.14	0.63	32.2
	Run A						0.60	30.5
	Run D						0.60	30.5

[a] Surface area per gram of catalyst.
[b] Surface area per gram of metal.

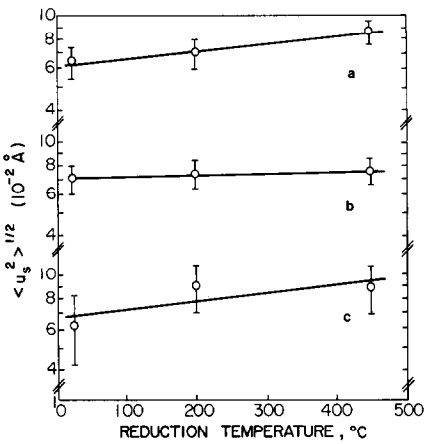

FIG. 10. Root-mean-square vibrational amplitudes of Pt vs reduction temperature. (a) D_h = 6.3%, (b) D_h = 21.5%, (c) D_h = 40%.

creases for all sizes, but plotting this vs the vibrational amplitude, Fig. 11, does not reveal any simple relationship.

CONCLUSIONS

(1) For $D_h \leq 40\%$, Pt catalysts exposed to air consist of metallic particles covered with a layer of adsorbed oxygen which does not change the geometry of the Pt core.

(2) For $D_h \leq 40\%$, exposure to air or to H_2 reduction does not alter the Pt–Pt nearest-neighbor distance.

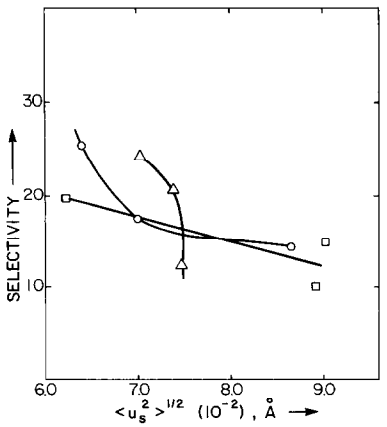

FIG. 11. Selectivity from Fig. 6 vs rms vibrational amplitude from Fig. 10. ○: D_h = 6.3%; △: D_h = 21.5%; □: D_h = 40%.

(3) For $D_h > 40\%$, the particles of catalyst stored in air are largely crystalline Pt_3O_4.

(4) For Pt with D_h = 6.3%, H_2 reduction causes a decrease in particle size and the new smaller particles are not chemically active.

(5) Increasing the temperature of reduction increases the vibrational amplitude, and this correlates with selectivity.

(6) To characterize properly highly dispersed catalysts, EXAFS studies should be combined with other tools, such as WAXS.

ACKNOWLEDGMENTS

This research was sponsored by DOE under Grant DE-ACO2-77ERO-4254. The diffraction studies with laboratory sources were carried out in the X-ray facility of Northwestern University's Materials Research Center, funded in part by NSF under Grant DMR-MRL-76-80847. We acknowledge the advice and assistance of Drs. D. H. Bilderback and D. Mills at CHESS (Cornell University), always given graciously. Dr. P. Georgopoulos (Northwestern University) advised us on EXAFS, Mr. R. Pahl assisted in processing the SAXS data, and T. K. Chuang obtained the results on chemical reactivity. Dr. E. Hall (Motorola Company) kindly provided the Si slices employed as monochromators in WAXS at CHESS.

REFERENCES

1. Uchijima, T., Herrmann, J. M., Inoue, Y., Burwell, R. L., Jr., Butt, J. B., and Cohen, J. B., *J. Catal.* **50,** 464 (1977).
2. Sashital, S. R., Cohen, J. B., Burwell, R. L., Jr., and Butt, J. B., *J. Catal.* **50,** 479 (1977).
3. Otero-Schipper, P. H., Wachter, W. A., Butt, J. B., Burwell, R. L., Jr., and Cohen, J. B., *J. Catal.* **50,** 494 (1977).
4. Inoue, Y., Herrmann, J. M., Schmidt, H., Burwell, R. L., Jr., Butt, J. B., and Cohen, J. B., *J. Catal.* **53,** 401 (1978).
5. Otero-Schipper, P. H., Wachter, W. A., Butt, J. B., Burwell, R. L., Jr., and Cohen, J. B., *J. Catal.* **53,** 414 (1978).
6. Bassi, I. W., Lytle, F. W., and Parravano, G., *J. Catal.* **42,** 139 (1976).
7. Joyner, R. W., *J. Chem. Soc. Faraday Trans. 1* **76,** 357 (1980).
8. Renouprez, A., Fouilloux, P., and Moraweck, B., *in* "Growth and Properties of Metal Clusters" (J. Bourdon, Ed.), p. 421. Elsevier, Amsterdam, 1980.
9. Borodzinski, A., and Janko, A., *React. Kinet. Catal. Lett.* **7,** 163 (1977).

10. Nandi, R., Pitchai, R., Wong, S. S., Cohen, J. B., Burwell, R. L., Jr., and Butt, J. B., *J. Catal.* **70,** 298 (1981).
11. Cullity, B. D., "Elements of x-Ray Diffraction," 2nd ed., Chap. 14. Addison–Wesley, Reading, Mass., 1978.
12. Ibers, J. A., and Hamilton, W. C. (Eds.), "International Tables for x-Ray Crystallography," Vol. 4. Kynoch Press, Birmingham, England, 1974.
13. Otero-Schipper, P. H., Ph.D dissertation, Northwestern University, Evanston, Ill., 1977. (Available from University Microfilms, Ann Arbor, Mich.)
14. Wong, S. S., Ph.D dissertation, Northwestern University, Evanston, Ill., 1980. (Available from University Microfilms, Ann Arbor, Mich.)
15. Goodisman, J., Brumberger, H., and Cupelo, R., *J. Appl. Crystallogr.* **14,** 305 (1981).
16. Winick, H., and Doniach, S. (Eds.), "Synchrotron Radiation Research," Chaps. 10–13. Plenum, New York, 1980.
17. Teo, B. K., and Joy, D. C. (Eds.), "EXAFS Spectroscopy: Techniques and Applications," Plenum, New York, 1981.
18. Teo, B. K., and Lee, P. A., *J. Amer. Chem. Soc.* **101,** 2815 (1979).
19. Muller, O., and Roy, R., *J. Less Common Met.* **16,** 129 (1968).
20. Moore, W. J., and Pauling, L., *J. Amer. Chem. Soc.* **63,** 1392 (1941).
21. Hecq, M., and Hecq, A., *J. Less Common Met.* **56,** 133 (1977).
22. Siegel, S., Hoekstra, H. R., and Tani, B. S., *J. Inorg. Nucl. Chem.* **31,** 3803 (1969).
23. Greegor, R. B., and Lytle, F. W., *J. Catal.* **63,** 476 (1980).
24. Sinfelt, J. J., Via, G. H., and Lytle, F. W., *J. Chem. Phys.* **68**(4), 200 (1978).